OCEANOGRAPHY

First global observations of third-degree ocean tides

Richard D. Ray

The Moon's tidal potential is slightly asymmetric, giving rise to so-called third-degree ocean tides, which are small and never before observed on a global scale. High-precision satellite altimeters have collected sea level records for almost three decades, providing a massive database from which tiny, time-coherent signals can be extracted. Here, four third-degree tides are mapped: one diurnal, two semidiurnal, and one terdiurnal. Aside from practical benefits, such as improved tide prediction for geodesy and oceanography, the new maps reveal unique ways the ocean responds to a precisely known, but hitherto unexplored, force. An unexpected example involves the two semidiurnals, where the smaller lunar force is seen to generate the larger ocean tide, especially in the South Pacific. An explanation leads to new information about an ocean normal mode that spatially correlates with the third-degree astronomical potential. The maps also highlight previously unknown shelf resonances in all three tidal bands.

INTRODUCTION

The Moon's gravitation induces a tidal potential at Earth's surface, which takes the well-known form of a two-sided tidal bulge. The spatial dependence of the potential can be expressed (1) in terms of spherical harmonic functions $Y_n^m(\varphi, \lambda)$, with latitude φ and longitude λ. Almost all common, day-to-day discussions of ocean tides refer to those waves excited by the degree $n = 2$ terms of the potential. These include the dominant semidiurnal tides (from Y_2^2), the diurnal tides (from Y_2^1), and the long-period tides (from Y_2^0), the latter having periods between a week and 18.6 years (2). The tidal bulge, however, is not perfectly symmetric, the side opposite the Moon being slightly weaker than the side with the Moon. The asymmetry gives rise to higher spherical harmonics in the tidal potential, most notably of degree $n = 3$. Since each term in the potential decays with distance from the Moon according to $\xi^{(n+1)}$, with ξ the Moon's parallax (about $^1/_{60}$), these third-degree tides are very small, roughly 60 times smaller than the common second-degree tides. Third-degree tides have been noticed occasionally in tide gauge records when many years of hourly data are carefully analyzed (3–6), but they have never been observed and mapped across the whole ocean.

The most accurate global tidal atlases (of second-degree tides) are based on numerical ocean models constrained by satellite altimetry (7). The orbits of the Topex/Poseidon and Jason satellites were specially designed for mapping major tidal constituents, and the many years of data from these and other altimeter missions have resulted in models now capable of predicting the open ocean tide with accuracies approaching 1 cm (8). It turns out that, as reported here, these many years of data are now sufficient to observe, with rather heavy smoothing, the subcentimeter third-degree tides.

An attempt to extract third-degree tides from altimetry should obviously focus on those constituents with the largest potential. Those are listed in Table 1 (9). The nomenclature for these tides has never been standardized; here, I use a preceding superscript "3" to distinguish the third-degree tides from standard second-degree tides. (A superscript for M_3 is superfluous since there can be no second-degree tides in the terdiurnal band, just as there is no Y_2^3 spherical harmonic.) The equilibrium tides ζ_{EQ} (fig. S1) have maximum elevations between only 1.1 and 2.6 mm. The ocean's dynamic response

NASA Goddard Space Flight Center, Greenbelt, MD 20771, USA.
Corresponding author. Email: richard.ray@nasa.gov

is expected to be considerably larger than equilibrium, however, just as it is for second-degree tides.

All the constituents in Table 1 except M_3 have frequencies that differ from much larger second-degree tides by only one cycle in 8.85 years (the precession period of the Moon's perigee). Thus, any study of third-degree tides requires many years of observations, merely for signal separation. Moreover, small tidal amplitudes, suggested by the equilibrium calculations, similarly necessitate many years of data to overcome low signal to noise. With the Topex/Poseidon-Jason satellite time series now approaching three decades, it is timely to investigate whether this massive amount of altimetry is sufficient to detect and map these tiny signals.

RESULTS

The approach I have taken to extract third-degree tides is a straightforward extension of standard empirical tide mapping methods long used for satellite altimetry (see Materials and Methods) (10). The resulting amplitudes of the four estimated constituents (Fig. 1) are shown with minimal spatial smoothing to gauge general noise levels. Estimated phases tend to be somewhat erratic for these small amplitudes, but after fairly heavy smoothing, both amplitudes and phases lead to global charts (fig. S2) that appear geophysically reasonable: long wavelengths throughout major ocean basins, with multiple amphidromic features, and shorter wavelengths with higher amplitudes on continental shelves. In that sense, they mimic familiar charts of conventional second-degree tides (2). In their details, however, the new charts look nothing like conventional charts owing to the very different tidal forcings.

For example, conventional diurnal tides are relatively suppressed throughout the whole Atlantic Ocean, whereas $^3M_1$ is seen to be relatively large in the North Atlantic. Cartwright (3) had already noticed this from tide gauge observations on the northwest European Shelf, finding that the amplitude of $^3M_1$ even exceeded that of the second-degree M_1. The altimetry shows that $^3M_1$ reaches even higher amplitudes in the northwest Indian Ocean (although in that region, M_1 remains larger). Compared with its amplitudes in the Atlantic and Indian oceans, $^3M_1$ is small in the Pacific, especially the South Pacific where it fails to reach even 2 mm. This can also be seen in Pacific island tide gauges, as recently reported by Woodworth (11). There are isolated $^3M_1$ shelf resonances that merit future attention, such as the upper Okhotsk Sea, the far southern Patagonian Shelf,

Table 1. Third-degree tidal constituents. The (extended) Doodson number (*2*) unambiguously defines the tidal arguments in terms of conventional astronomical parameters. The maximum equilibrium tide ζ_{EQ} is generally much smaller than the actual dynamic ocean tide, but it is a proper measure of the strength of the astronomical forcing (*9*). It has been scaled by the Love number combination $(1 + k_3 - h_3) = 0.802$ to account for the presence of the body tide (*40*). The maximum observed tide $\zeta_{observed}$ is a lower bound for the first three, since the altimetry likely misses the peaks of any shelf resonances; but the observed maximum in M_3 is based on a coastal tide gauge (*13*).

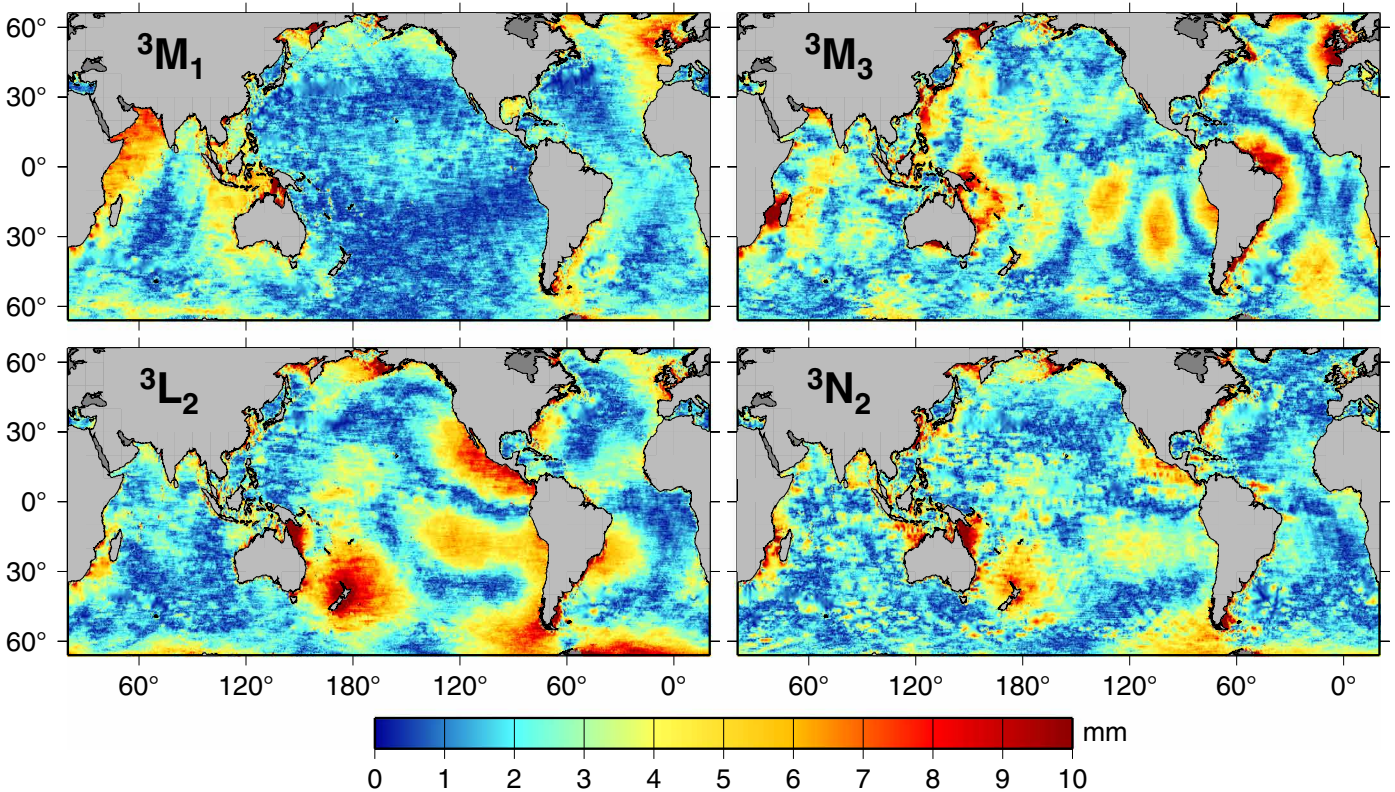| Constituent	Frequency (°/hour)	Period (hour)	Doodson argument	Max ζ_{EQ} (mm)	Max $\zeta_{observed}$ (mm)
$^3M_1$	14.492052	24.8412	155.5552	1.424	28 (south coast of Papua)
$^3N_2$	28.435088	12.6604	245.5551	1.227	32 (Bristol Bay, Alaska)
$^3L_2$	29.533121	12.1897	265.5553	1.133	49 (Bristol Bay, Alaska)
$^3M_3$	43.476156	8.2804	355.5552	2.560	158 (Paranagua, Brazil)

Fig. 1. Amplitudes of estimated third-degree tides from satellite altimetry. Minimal smoothing has been applied, other than from overlapping analysis bins. Effects of solid Earth tides, both body tides and crustal load tides, have been removed (*41*). Latitude limits (±66°) are defined by the Topex-Jason orbit coverage. In a few locations, the amplitudes considerably exceed the color scale, especially for a handful of M_3 shelf resonances (*13*).

and Norton Sound off western Alaska, but according to the altimeter solutions, the largest amplitudes occur in a localized resonance off the southern coast of Papua (Western New Guinea), where $^3M_1$ reaches at least 28 mm. There are unfortunately no tide gauges in that region to check this. There is a single, fairly new, tide gauge in the interior of Norton Sound at Unalakleet (Alaska), but the time series is, so far, too short to separate M_1 and $^3M_1$.

M_3 (or $^3M_3$) has a few open-ocean regions where it reaches amplitudes of about 5 mm and even larger off northeast Brazil, but otherwise, its largest amplitudes are more closely confined to the marginal seas and continental shelves. On the basis of a large array of bottom pressure data, Cartwright *et al.* (*12*) produced a hand-drawn cotidal chart of M_3 for the northeast Atlantic, which showed large amplitudes off Britain and in the Bay of Biscay and very low amplitudes

farther to the west (near 25°W); the altimetry nicely confirms their chart (Fig. 1 and fig. S2 even place a large, elongated low close to where Cartwright drew a double amphidrome). From other past tide gauge observations, there are known shelf resonances where M_3 reaches unusually large amplitudes: 150 mm on the wide shelf off Paranagua, Brazil (*13*) and over 100 mm along part of the South Australian Bight (*14*). The altimetry picks up these same short-scale features, and it also reveals large amplitudes, well over 10 mm, along the entire Madagascar Channel.

The two semidiurnal tides reach their largest amplitudes in a shelf resonance in Bristol Bay (southwest Alaska). There are also strong amplitudes surrounding New Zealand as well as across the whole Coral Sea, where the waves are abruptly stopped in the west by Torres Strait. The two semidiurnals are discussed in more detail below.

There have been at least two attempts to simulate third-degree ocean tides by numerically solving the tidal hydrodynamic equations on a global grid, notably three decades ago by Platzman (15) who computed $^3N_2$ and $^3M_1$, and more recently by Woodworth (11) who computed $^3M_1$. Both efforts were unconstrained by any observations. We are now in a position to examine how realistic those simulations were. Platzman's early work was based on a very coarse finite-element grid, and it could not capture the large $^3N_2$ amplitudes that altimetry detects in the Coral Sea, but there is otherwise some qualitative agreement in our charts. The most conspicuous feature in his semidiurnal map was a large Kelvin wave around Antarctica. This wave likely exists, but it must be more closely confined to the continent than what Platzman's chart depicted, and outside the 66°S limits of Fig. 1. There is also reasonable qualitative agreement in $^3M_1$, although Platzman obtained his largest amplitudes by far in the northeast Atlantic. Qualitative agreement with Woodworth's $^3M_1$ simulation is even more encouraging. Minor shifts in the locations of amphidromes are apparent, but that is expected. Woodworth had largest amplitudes off northwest Australia where the altimetry also detects relatively large amplitudes, but not nearly so large as in the northwest Indian Ocean. Both Platzman and Woodworth find a diurnal Antarctic Kelvin wave, which again must be mostly below 66°S.

Applications

Global tidal models have widespread applications throughout oceanography and geodesy (16). Before examining in more detail an interesting aspect of the ocean's response to the third-degree forcing, it is worth highlighting a few applications that can be anticipated for these new tidal charts.

Tidal prediction

Practical tide prediction of ocean sea surface heights is perhaps the most common application of regional and global models. Prediction normally benefits from additional constituents, so long, of course, as they are accurate. Most national agencies responsible for tide prediction at major ports do include M_3, deducing it from past observations at a tide gauge (17). However, neither M_3 nor any other third-degree tide is ever included in open-ocean tide prediction simply owing to a lack of global models. It is obvious that for a large coastal shelf resonance—for example, the 10-cm resonance in M_3 along the Great Australian Bight—it is important to include that constituent in prediction. It is less obvious that prediction elsewhere benefits from the other tides considered here. The small error of omission may be overwhelmed by errors from other sources, such as errors in the major tide constituents, possibly making third-degree tides irrelevant to prediction. Two examples show that this is not the case for at least some open-ocean locations.

Two bottom pressure recorders of the international tsunami warning network (18) are in locations where third-degree tides approach or exceed 1-cm amplitudes: station 23228 in the Arabian Sea and station 43412 in the eastern Pacific off Mexico. Adopting the global tide model FES2014 [an update of (19)] for second-degree constituents, I computed tide predictions for these two stations with and without the additional new third-degree tides. The prediction error was computed by subtracting the predicted tide from the observed bottom pressure and by (generously) assuming that all variability at frequencies greater than 0.6 cycles per day was associated with tides; see (8) for details. The root mean square (RMS) prediction errors for the two stations were 1.87 ± 0.07 and 1.15 ± 0.08 cm, respectively, without the new constituents, and 1.65 ± 0.06 and 0.97 ± 0.05 cm with

them, where the uncertainty is the standard deviation computed from many independently processed months of data. Although small, the third-degree tides yield a significant reduction in prediction error.

The same methodology was applied to the tide gauge at Cape Ferguson, located on the coast of Queensland, Australia, where the third-degree semidiurnals are relatively large. The tide prediction error was 4.88 ± 0.40 cm without and 4.36 ± 0.40 cm with the new constituents. Coastal tide gauges represent a more difficult case, since other errors come into play, such as the existence of nonlinear compound tides, yet at this Australian site, the new constituents do result in a good reduction in prediction error.

Earth tides

The third-degree terms in the lunar potential also induce third-degree Earth tides (20). A long multiyear time series is still required to separate the close frequencies of second- and third-degree tides. Using the global network of superconducting gravimeters (21), Ducarme (22) successfully extracted and studied third-degree Earth tide signals at 17 sites. An important goal of Earth tide studies, including Ducarme's, is to refine models of Earth's deep elastic (or anelastic) response. His conclusion was: "To take a decisive step forward in the selection of the optimal [Earth] model, it should be necessary to have ocean tide models for the waves deriving from the third degree potential." The work presented here provides a first-generation set of these models, and for the same four constituents studied by Ducarme.

Ocean tides perturb Earth-tide gravity measurements in two ways: by direct Newtonian attraction of the ocean mass and by effects associated with crustal loading and deformation. Both effects can be computed efficiently over the entire globe by a spherical harmonic approach (23). Results for our four constituents are shown in fig. S3. The largest gravity perturbation, with an amplitude of approximately 2.0 nm/s^2, occurs in M_3 near the large shelf resonance off Brazil (13).

An example suffices to establish the value of these ocean models for Earth tide work. The most anomalous result observed by Ducarme (22) was his estimate for $^3M_1$ at Canberra, Australia. In terms of the Love number combination $\delta = (1 + 2h_3/3 − 4k_3/3)$, Ducarme obtained a value of 1.109 ± .004, whereas most theoretical Earth models are in the range of 1.069 to 1.073. He also obtained an anomalously large phase of −4.18 ° ± 0.22°, whereas the theoretical phase is very small, a fraction of a degree. Using the data of fig. S3, I adjusted Ducarme's observed estimate to obtain an ocean-corrected value of $\delta = 1.071$, with phase 0.36°, which is now consistent with theory. Ducarme had already noted that his cluster of 11 European stations had a mean δ of 1.0827, which is 1% higher than any theoretical Earth model; for the ocean-corrected version of his data, I find a mean δ for the European stations of 1.0718, now again more consistent with theory.

Satellite gravimetry

For satellite gravity missions such as GRACE (Gravity Recovery and Climate Experiment) and GRACE Follow-On (24) tidal models are a critical a priori component for dealiasing the measured satellite-to-satellite ranging data. Errors in tidal models are suspected of being one of the largest—if not the largest—error sources in satellite gravity solutions (25). One useful way to detect the presence of tide modeling errors is to examine GRACE range-rate measurement residuals as a function of location and to check for the presence of significant energy at tidal frequencies (26). When this is done, some clear effects of the neglected third-degree tides do appear. An example (Fig. 2) for M_3 shows residual energy (in terms of range acceleration) appearing over locations where the altimeter maps indicate
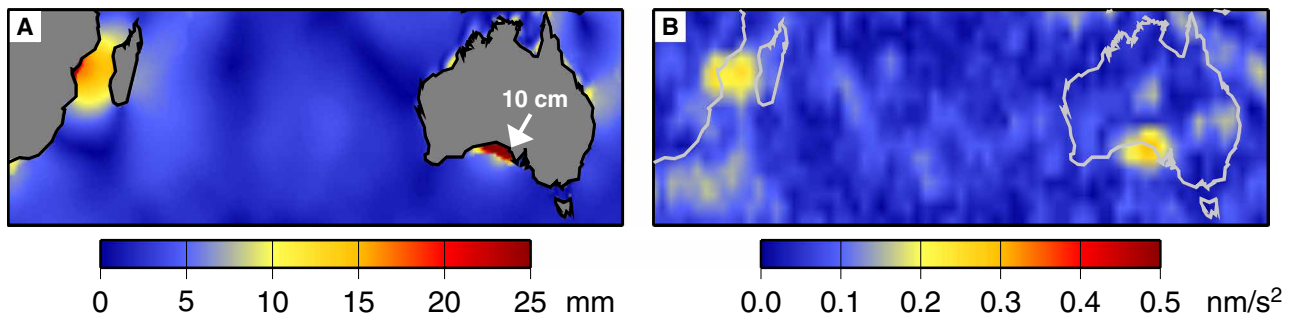
Fig. 2. Errors in satellite gravimetry caused by neglected modeling of the $^3M_3$ tide. (**A**) Zoomed view of the $^3M_3$ ocean tide estimated from satellite altimetry, corresponding to the smoothed solution in fig. S2. (**B**) Amplitudes of mismodeling errors in GRACE satellite-to-satellite range acceleration at the $^3M_3$ frequency, showing errors colocated with the largest signals observed in (A). The acceleration residuals were computed along (essentially north-south) satellite tracks from data collected during 2004–2010. Examination of these residuals is a useful way of detecting the presence of tide modeling errors, although in a qualitative way since results are in terms of satellite acceleration (26). Future incorporation of third-degree tides in GRACE reprocessing should reduce or eliminate these errors.
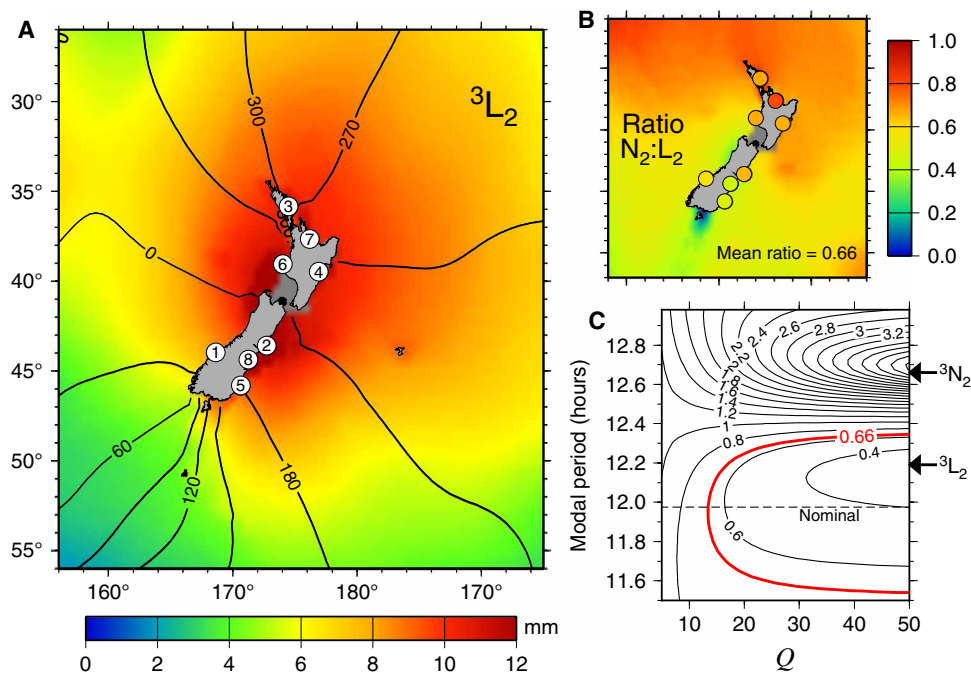

Fig. 3. Third-degree semidiurnal tides around New Zealand and implied single-mode period and Q. (**A**) Cotidal chart of $^3L_2$ showing amplitudes in color and iso-phase contour lines every 30°. Eight New Zealand tide gauges are labeled as used in table S1. (**B**) Ratio of $^3N_2$ to $^3L_2$ amplitudes. The mean ratio over the whole region is 0.66. (**C**) Theoretical ratio of $^3N_2$ to $^3L_2$ amplitudes when both are synthesized from a single oceanic normal mode, as a function of the modal period and quality factor Q. Red contour line is the ratio of 0.66, as given in (B). Müller's calculated eigenperiod (28) of this mode is 11.97 hours, implying a modal Q of about 14.

relatively large M_3 amplitudes. Other third-degree tides have similar signals in GRACE residuals. Future GRACE data reprocessing can thus be expected to benefit from incorporation of third-degree ocean tide models into the necessary suite of prior dealiasing models.

Semidiurnal responses and normal modes

A most unexpected result in the new tidal charts concerns the two semidiurnal constituents $^3N_2$ and $^3L_2$. Throughout the Pacific and Atlantic oceans, $^3L_2$ is, by far, the larger of the two although (Table 1) it has the slightly weaker astronomical forcing. For example, consider the large tidal amplitudes around New Zealand (Fig. 3A) where the signal-to-noise levels are relatively high. In that region, the mean ratio of $^3N_2$ to $^3L_2$ amplitudes is about 0.66 (Fig. 3B). The remainder

of this section develops an explanation for this unusual fact, which leads to new insight, or confirmations, concerning the ocean's barotropic normal modes and their properties.

In a normal-mode viewpoint, the complex tidal elevations $\zeta_\omega(x)$ of a constituent of frequency ω is expanded in a series of modes $Z_k(x)$ as (27)

$$\zeta_\omega(x) = C(\omega) \sum_k (1 - \omega/\sigma_k)^{-1} S_k Z_k(x) \qquad (1)$$

where the coefficient $C(\omega)$ is proportional to the constituent's astronomical potential, so a tidal "admittance" can be expressed as ζ/C. The admittance is then a function of three factors: a frequency factor depending only on ω and its nearness to the modal frequencies σ_k; a
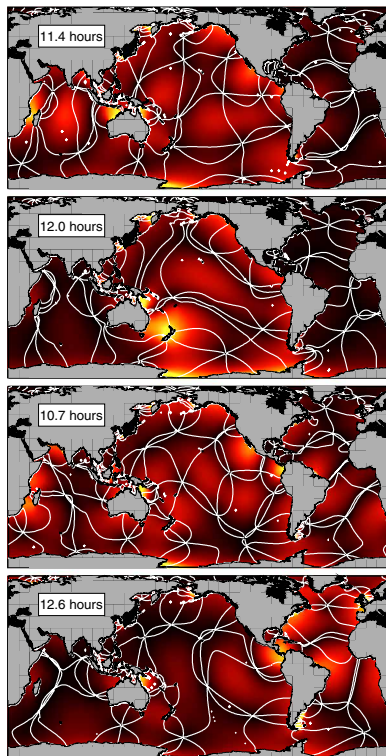
Fig. 4. Ocean normal modes most coherent with Y_3^2 astronomical potential.
Modes were computed by Müller (28) for the global ocean, who found 21 modes in or near the semidiurnal tidal band. Of these, the four shown here have the highest spatial coherence with the third-degree semidiurnal astronomical potential. The second-highest coherence is the 12-hour mode, which dominates the large semidiurnal ocean response around New Zealand, as seen in Fig. 1. Scaling of modal amplitudes (in color) is arbitrary; phase lines are shown every 60°.

shape factor S_k that depends on the spatial coherence between the astronomical potential and each modal elevation; and the complex modal elevations Z_k themselves, evaluated at location x.

The most definitive set of oceanic normal modes is currently those computed by Müller (28). They supersede the well-known pioneering efforts by Platzman et al. (29), thanks to much finer spatial resolutions and by accounting for wave self-attraction and crustal loading effects. In the near-semidiurnal band, with periods between 10 and 15 hours, Müller found 21 eigenmodes in his numerical ocean. I computed the spatial coherence S_k between each of these modes and the semidiurnal Y_3^2 potential. This then identifies those modes that are likely to be most important in defining the ocean's tidal response. The four modes of highest coherence have periods of 11.38, 11.97, 10.70, and 12.65 hours (with S_k in the proportions 1.00, 0.88, 0.58, and 0.56, respectively, so the first two modes dominate). These four modes are shown in Fig. 4. The 11.97-hour mode is localized to New Zealand and northeast Australia and is nearly zero in the Atlantic and Indian oceans. Although all modes contribute, more or less, to the tide at any given location, the semidiurnal tide around New Zealand appears to be dominated by the single mode of period 11.97 hours, as the other three modes are small there.

To the extent that the resonant-like feature around New Zealand is indeed dominated by the single 11.97-hour mode, it is immediately evident why $^3L_2$ is so much larger than $^3N_2$: The 11.97-hour period is much closer to the period of $^3L_2$ (Table 1), so the frequency factor

in Eq. 1 favors a magnified $^3L_2$ over $^3N_2$. This point can be made more quantitative.

The period T and specific dissipation Q^{-1} of a normal mode are directly related (27, 30) to the mode's complex frequency σ by $T = 2\pi/$ Re σ and $Q^{-1} = 2$ Im σ/ Re σ. Both were determined in the original (28) eigenmode calculations, but for the sake of argument, T and Q can be treated as free parameters. The theoretical ratio of the $^3N_2$ to $^3L_2$ amplitudes may be evaluated by Eq. 1 in terms of T, Q. The results are shown in Fig. 3C. The red contour line follows the ratio 0.66, which is the value deduced from the altimeter tide solutions for the region around New Zealand (Fig. 3B). Figure 3C implies that the normal mode would need a period of approximately 12.4 hours or longer, almost independent of its Q, before the N:L ratio could follow the astronomical potential and take a value near or greater than 1. For the mode's nominal period of 11.97 hours, the observed ratio of 0.66 implies that Q is about 14. This Q is not far different from what has been previously reported for the (second-degree) semidiurnal tides of the North Atlantic (27, 31, 32). The implied exponential time constant $\tau = 2Q/\omega$ is 54 hours, slightly smaller than the 68 hours found for this mode by Müller from his numerical ocean model with linearized friction.

To the extent that the real ocean can be approximated by a linear barotropic model, a set of global oceanic normal modes must exist, although they have always seemed curiously concealed (33), presumably by the ocean's many broadband forced motions and its high dissipation. Several decades ago, Platzman (27) summarized three lines of evidence, all based on consideration of tidal admittances, indirectly supporting the existence and the characteristics of ocean modes. Evidence for modal excitation by broadband atmospheric forcing has been more elusive but has been detected in bottom pressure and other measurements in the Southern Ocean (34, 35). The third-degree semidiurnal tides explored here add to this line of evidence, and in addition, they support the eigenanalysis computed by Müller (28) for both the structure and the period of the 12-hour mode, a mode not so evident in Platzman's earlier work, probably owing to its coarse spatial resolution.

DISCUSSION

Mapping third-degree tides across the global ocean is possible only because we now have nearly three decades of high-quality satellite altimetry. With massive averaging of these data, the third-degree waves, of amplitudes no more than a few millimeters in most places, gradually emerge from the background. The terdiurnal tide M_3 rises to significantly greater amplitudes (over 10 cm) at a few shelf resonances, such as along the Great Australian Bight.

Even with three decades of data, the altimeter-based maps are noisy, which is expected in light of the small amplitudes of the signals. An important next step will be to replace the ad hoc smoothing methods used here with more formal inverse methods, allowing assimilation of the altimeter data into numerical hydrodynamic ocean models (36). This should result in more accurate maps and should especially help refine the large amplitudes of shelf and coastal resonances where the resolution of altimetry tends to be limited. These largest amplitudes are, of course, the most important for many applications.

The ocean's response to the third-degree terms of the Moon's gravitational potential, yielding ocean tides that look nothing like familiar tides from the second-degree terms, opens new opportunities for in-depth investigation. The modal response considered here for the two semidiurnal constituents is but one example. Moreover,

the success of satellite altimetry in extracting these tiny waves suggests further possibilities, such as mapping of open-ocean nonlinear tides (37) to study how these waves, propagating freely from sources in shallow water, radiate and dissipate. Tiny climate-induced changes in tides (38) may also begin rising above background noise levels in altimetry. It is yet another example of the dictum that aiming for measurements of ever-higher precision is a prescription for progress in the natural sciences. For tides, the longer the time series, the finer the precision.

MATERIALS AND METHODS

The satellite altimeter data used in this investigation have been obtained from (and partially processed by) the Radar Altimeter Database System (39). All data used throughout the deep, open ocean are from the satellite missions Topex/Poseidon, Jason-1, Jason-2, and Jason-3. The ground tracks for these missions are too widely spaced to adequately map smaller-scale tidal features common in shallow seas. So, for shallow water regions only, these primary data have been supplemented with altimeter measurements from missions ERS-2, Envisat, SARAL, Geosat Follow-On, and Sentinel-3A.

The tidal analysis followed conventional empirical approaches (10). Data were compiled into small overlapping geographical bins covering the ocean surface, and the data in each bin were independently subjected to tidal analysis. Bin sizes were variable, depending on water depth and nearby coastlines. Because the goal here was to extract tides of unusually small amplitude, the deep-ocean bins were fairly large, covering up to 6° of longitude and 2° of latitude.

Since all estimated constituents are of lunar origin, they are all modulated by the precession of the Moon's orbit plane. This is generally handled by allowing for an a priori amplitude modulation f and phase modulation u. I have worked these out from the astronomical potential (9). Conventional series expansions are given in table S2. Constituent $^3N_2$ is more complicated, because it is also modulated by motion of the Moon's perigee, leading to equations given in the table caption. Over the course of 18.6 years, the diurnal $^3M_1$ experiences the largest amplitude modulation: ±28%. The semidiurnal $^3L_2$ has the largest phase modulation: ±14°.

The third-degree body tides were removed from the altimeter measurements using the Love number $h_3 = 0.291$ (40). The tidal analysis thus solved for a combined ocean + load tide, and the load tide was subsequently estimated and removed via an iterative algorithm (41) in a center-of-mass reference frame (42).

Very small tidal signals are difficult to extract in regions of high mesoscale variability, so these regions (Gulf Stream, Kuroshio, etc.) were masked and the solutions interpolated across them. Otherwise, the raw tidal estimates obtained are as depicted in Fig. 1.

Tide gauge comparisons

A test of the altimeter tide solutions was conducted by comparing tidal constants with those computed from a set of globally distributed tide gauges. For this exercise, island gauges have been favored since altimetry is most accurate over the open ocean away from land contamination.

I used a selection of 99 tide gauges taken from the Global Extreme Sea Level Analysis version 2 (GESLA-2) database (43) of hourly sea level measurements. The original database contains 1276 stations, but a number of these are duplicates or otherwise unsatisfactory for the present application. In addition to selecting mainly island gauges, all accepted stations were required to have at least nine full years of data (to separate second-degree from third-degree constituents) and have data collected during the past three decades (when time-keeping errors were less likely). The distribution of the 99 stations is shown in fig. S4.

The RMS differences between the tide gauge constants and the altimeter results (Fig. 1) and the smoothed altimeter results (fig. S2) are given in Table 2. Both altimeter results show a reduction in variance relative to the tide gauge signal, but the smoothed versions account for much greater, and indeed a substantial, amount of the tide gauge variance. Of course, the tide gauge estimates themselves are not perfect, so some residual variance is inescapable. These comparison statistics suggest that the altimeter results represent a fair depiction of the third-degree constituents.

A more detailed comparison that focuses only on the semidiurnal constituents at eight tide gauges around New Zealand (Fig. 3A) is given in table S2. The tide gauges confirm the unexpected altimeter result: an enhancement of $^3L_2$ in that region relative to $^3N_2$, although $^3N_2$ has the larger forcing.

SUPPLEMENTARY MATERIALS

Supplementary material for this article is available at http://advances.sciencemag.org/cgi/content/full/6/48/eabd4744/DC1

REFERENCES AND NOTES

1. P. Melchior, *The Earth Tides* (Pergamon Press, 1966).
2. D. T. Pugh, P. L. Woodworth, *Sea Level Science: Understanding Tides, Surges, Tsunamis and Mean Sea-Level Changes* (Cambridge Univ. Press, 2014).
3. D. E. Cartwright, A subharmonic lunar tide in the seas off western Europe. *Nature* **257**, 277–280 (1975).
4. G. Godin, G. Gutierrez, Third order effects in the tide of the Pacific, near Acapulco. *Deep Sea Res.* **32**, 407–415 (1985).
5. D. E. Cartwright, R. Spencer, J. M. Vassie, P. L. Woodworth, The tides of the Atlantic Ocean, 60°N to 30°S. *Phil. Trans. R. Soc. A* **324**, 513–563 (1988).
6. R. D. Ray, Resonant third-degree diurnal tides in the seas off Western Europe. *J. Phys. Oceanogr.* **31**, 3581–3586 (2001).
7. D. Stammer, R. D. Ray, O. B. Andersen, B. K. Arbic, W. Bosch, L. Carrère, Y. Cheng, D. S. Chinn, B. D. Dushaw, G. D. Egbert, S. Y. Erofeeva, H. S. Fok, J. A. M. Green, S. Griffiths, M. A. King, V. Lapin, F. G. Lemoine, S. B. Luthcke, F. Lyard, J. Morison, M. Müller, L. Padman, J. G. Richman, J. F. Shriver, C. K. Shum, E. Taguchi, Y. Yi, Accuracy assessment of global barotropic ocean tide models. *Rev. Geophys.* **52**, 243–282 (2014).
8. R. D. Ray, G. D. Egbert, Tides and satellite altimetry, in *Satellite Altimetry Over Oceans and Land Surfaces*, D. Stammer, A. Cazenave, Eds. (CRC Press, 2018), chap. 13, pp. 427–458.

Table 2. Tide comparison statistics: Altimetry versus tide gauges. RMS signal (in millimeters) in tide gauges and RMS differences (in millimeters) between altimeter tide solutions and 99 "ground truth" tide gauges. The tide gauges are a selection of mostly island locations (fig. S4) with long time series, taken from the GESLA-2 database (43). The "raw charts" refer to those in Fig. 1; the "smoothed charts" refer to those in fig. S2.

Constituent	RMS signal (mm)	RMS diff. Raw charts	RMS diff. Smoothed charts
$^3M_1$	1.62	1.31	0.50
$^3N_2$	1.93	1.75	0.79
$^3L_2$	2.35	1.56	1.08
$^3M_3$	2.85	1.46	0.79

9. D. E. Cartwright, R. J. Tayler, New computations of the tide-generating potential. *Geophys. J. R. Astr. Soc.* **23**, 45–74 (1971).

10. E. J. O. Schrama, R. D. Ray, A preliminary tidal analysis of TOPEX/Poseidon altimetry. *J. Geophys. Res.* **99**, 24799–24808 (1994).

11. P. L. Woodworth, The global distribution of the M1 ocean tide. *Ocean Sci.* **15**, 431–442 (2019).

12. D. E. Cartwright, A. C. Edden, R. Spencer, J. M. Vassie, The tides of the northeast Atlantic Ocean. *Phil. Trans. R. Soc. Lond. A* **298**, 87–139 (1980).

13. J. M. Huthnance, On shelf-sea 'resonance' with application to Brazilian M3 tides. *Deep Sea Res.* **27**, 347–366 (1980).

14. P. A. Hutchinson, The physical characteristics of the ter-diurnal shelf resonance along the eastern Great Australian Bight, thesis, Flinders University of South Australia (1988).

15. G. W. Platzman, Normal modes of the world ocean. Part IV: Synthesis of diurnal and semidiurnal tides. *J. Phys. Oceanogr.* **14**, 1532–1550 (1984).

16. H. Wilhelm, W. Zürn, H.-G. Wenzel, *Tidal Phenomena* (Springer, 1997).

17. B. B. Parker, Tidal analysis and prediction (NOAA Special Publication NOS CO-OPS 3, National Oceanic and Atmospheric Administration, 2007).

18. G. Mungov, M. Eblé, R. Bouchard, DART® tsunameter retrospective and real-time data: A reflection on 10 years of processing in support of tsunami research and operations. *Pure Appl. Geophys.* **170**, 1369–1384 (2013).

19. F. Lyard, F. Lefevre, T. Letellier, O. Francis, Modelling the global ocean tides: Modern insights from FES2004. *Ocean Dynam.* **56**, 394–415 (2006).

20. P. Melchior, B. Ducarme, O. Francis, The response of the Earth to tidal body forces described by second- and third-degree spherical harmonics as derived from a 12 year series of measurements with the superconducting gravimeter GWR/T3 in Brussels. *Phys. Earth Planet. Inter.* **93**, 223–238 (1996).

21. D. Crossley, J. Hinderer, A review of the GGP network and scientific challenges. *J. Geodyn.* **48**, 299–304 (2009).

22. B. Ducarme, Determination of the main Lunar waves generated by the third degree tidal potential and validity of the corresponding body tides models. *J. Geod.* **86**, 65–75 (2012).

23. J. B. Merriam, The series computation of the gravitational perturbation due to an ocean tide. *Phys. Earth Planet. Inter.* **23**, 81–86 (1980).

24. F. W. Landerer, F. M. Flechtner, H. Save, F. H. Webb, T. Bandikova, W. I. Bertiger, S. V. Bettadpur, S. H. Byun, C. Dahle, H. Dobslaw, E. Fahnestock, N. Harvey, Z. Kang, G. L. H. Kruizinga, B. D. Loomis, C. McCullough, M. Murböck, P. Nagel, M. Paik, N. Pie, S. Poole, D. Strekalov, M. E. Tamisiea, F. Wang, M. M. Watkins, H.-Y. Wen, D. N. Wiese, D.-N. Yuan, Extending the global mass change data record: GRACE Follow-On instrument and science data performance. *Geophys. Res. Lett.* **47**, e2020GL088306 (2020).

25. F. Flechtner, N. K.-H. C. Dahle, H. Dobslaw, E. Fagiolini, J.-C. Raimondo, A. Güntner, What can be expected from the GRACE-FO laser ranging interferometer for earth science applications? *Surv. Geophys.* **37**, 453–470 (2016).

26. R. D. Ray, S. B. Luthcke, J.-P. Boy, Qualitative comparisons of global ocean tide models by analysis of intersatellite ranging data. *J. Geophys. Res.* **114**, C09017 (2009).

27. G. W. Platzman, Tidal evidence for ocean normal modes, in *Tidal Hydrodynamics*, B. B. Parker, Ed. (John Wiley & Sons, 1991), pp. 13–26.

28. M. Müller, The free oscillations of the world ocean in the period range 8 to 165 hours including the full loading effect. *Geophys. Res. Lett.* **34**, L05606 (2007).

29. G. W. Platzman, G. A. Curtis, K. S. Hansen, R. D. Slater, Normal modes of the world ocean. Part II: Description of modes in the period range 8 to 80 hours. *J. Phys. Oceanogr.* **11**, 579–603 (1981).

30. C. Garrett, Tidal resonance in the Bay of Fundy and Gulf of Maine. *Nature* **238**, 441–443 (1972).

31. C. Garrett, D. Greenberg, Predicting changes in tidal regime: The open boundary problem. *J. Phys. Oceanogr.* **7**, 171–181 (1977).

32. R. A. Heath, Estimates of the resonant period and Q in the semi-diurnal tidal band in the North Atlantic and Pacific Oceans. *Deep Sea Res.* **28**, 481–493 (1981).

33. D. S. Luther, Why haven't you seen an ocean mode lately? *Ocean Model.* **50**, 1–6 (1983).

34. R. M. Ponte, Propagating bottom pressure signals around Antarctica at 1–2-day periods and implications for ocean modes. *J. Phys. Oceanogr.* **34**, 284–292 (2004).

35. K. Kusahara, K. I. Ohshima, Kelvin waves around Antarctica. *J. Phys. Oceanogr.* **44**, 2909–2920 (2014).

36. G. D. Egbert, A. F. Bennett, Data assimilation methods for ocean tides, in *Modern Approaches to Data Assimilation in Ocean Modeling*, P. Malanotte-Rizzoli, Ed. (Elsevier, 1996), pp. 147–179.

37. R. D. Ray, Propagation of the overtide M4 through the deep Atlantic Ocean. *Geophys. Res. Lett.* **34**, L21602 (2007).

38. I. D. Haigh, M. D. Pickering, J. A. M. Green, B. K. Arbic, A. Arns, S. Dangendorf, D. F. Hill, K. Horsburgh, T. Howard, D. Idier, D. A. Jay, L. Jänicke, S. B. Lee, M. Müller, M. Schindelegger, S. A. Talke, S.-B. Wilmes, P. L. Woodworth, The tides they are a-changin': A comprehensive review of past and future nonastronomical changes in tides, their driving mechanisms, and future implications. *Rev. Geophys.* **57**, e2018RG000636 (2019).

39. R. Scharroo, RADS data manual, version 4.3.6 (Technical Report, Eumetsat & Tech. Univ. Delft, 2019).

40. J. M. Wahr, Body tides on an elliptical, rotating, elastic and oceanless earth. *Geophys. J. R. Astr. Soc.* **64**, 677–703 (1981).

41. D. E. Cartwright, R. D. Ray, Energetics of global ocean tides from Geosat altimetry. *J. Geophys. Res.* **96**, 16897–16912 (1991).

42. S. D. Desai, R. D. Ray, Consideration of tidal variations in the geocenter on satellite altimeter observations of ocean tides. *Geophys. Res. Lett.* **89**, 2454–2459 (2014).

43. P. L. Woodworth, J. R. Hunter, M. Marcos, P. Caldwell, M. Menéndez, I. Haigh, Towards a global higher-frequency sea level dataset. *Geosci. Data J.* **3**, 50–59 (2017).

Citation: R. D. Ray, First global observations of third-degree ocean tides. *Sci. Adv.* **6**, eabd4744 (2020).